

Electrical resistivity and metal-nonmetal transition in *n*-type doped 4H-SiC

Antonio Ferreira da Silva

Instituto de Física, Universidade Federal da Bahia, Campus Ondina 40210-340 Salvador, BA, Brazil

Julien Pernot*

*Laboratoire d'Etudes des Propriétés Electroniques des Solides (CNRS), 25 avenue des Martyrs, BP 166,**38042 Grenoble Cedex 9, France**and Université Joseph Fourier, BP 53, 38041 Grenoble Cedex 9, France*

Sylvie Contreras

Groupe d'Etude des Semiconducteurs, UM2-CNRS (UMR 5650), cc074, 34095 Montpellier, Cedex 5, France

Bo E. Sernelius

Department of Physics, Chemistry and Biology, Linköping University, SE-581 83 Linköping, Sweden

Clas Persson

Department of Materials Science and Engineering, Royal Institute of Technology, SE-100 44 Stockholm, Sweden

Jean Camassel

Groupe d'Etude des Semiconducteurs, UM2-CNRS (UMR 5650), CC074, 34095 Montpellier, Cedex 5, France

(Received 26 September 2006; published 5 December 2006)

The electrical resistivity of 4H-SiC doped with nitrogen is analyzed in the temperature range 10–700 K for nitrogen concentrations between 3.5×10^{15} and 5×10^{19} cm⁻³. For the highest doped samples, a good agreement is found between the experimental resistivity and the values calculated from a generalized Drude approach at similar dopant concentration and temperature. From these results, the critical concentration (N_c) of nitrogen impurities which corresponds to the metal-nonmetal transition in 4H-SiC is deduced. We find $N_c \sim 10^{19}$ cm⁻³.

DOI: [10.1103/PhysRevB.74.245201](https://doi.org/10.1103/PhysRevB.74.245201)

PACS number(s): 71.30.+h, 72.10.-d

I. INTRODUCTION

4H-SiC has long been recognized as a promising material for high-temperature, high-power, and high-frequency electronic devices with outstanding application range. This includes rf and microwave power amplifiers for cellular phone base stations and power conversion devices for hybrid vehicles applications¹ as well as field-effect gas sensors to reduce environmental pollution² or high-temperature Hall sensors for motor control applications.³ Whatever the final target, understanding in great detail the role of impurities like nitrogen, phosphorus, or aluminium on the electrical properties of the active layers is a prerequisite to improve performance. For instance, to develop high-temperature Hall sensors, a deep understanding of the transport properties in the low concentration range is needed. On the opposite, to manufacture low resistance sources and drains in field-effect transistors with high breakdown electric field (of ~ 3 MV/cm) a most important point is to better understand the electrical behavior of highly doped SiC samples.

Recently, the transport properties of 4H-SiC epitaxial layers have been described as a function of the temperature using the relaxation time approximation for nitrogen density (N_d) lower than $\sim 10^{18}$ cm⁻³.^{4,5} From these results, the room-temperature electrical resistivity for a low doped active layer was shown to vary from 50 Ω cm for a donor concentration $N_d = 10^{14}$ cm⁻³ – 50 m Ω cm for $N_d = 10^{18}$ cm⁻³.⁶ Unfortunately, the calculation was limited to the donor concentration

which corresponds to the metal-nonmetal (MNM) transition (this concentration being evaluated at about 5.6×10^{18} cm⁻³ by Persson and co-workers for 4H-SiC polytype^{7,8}). Above this critical value, no calculation of the electrical resistivity was presented.

In this work, we focus on the resistivity of heavily nitrogen-doped 4H-SiC samples (4H-SiC:N) in the temperature range 10–700 K for impurity concentrations which span the semi-insulating to quasimetallic behaviors (3.5×10^{15} to 5×10^{19} cm⁻³). The experimental values of the sample's resistivity are then compared with the values computed from a generalized Drude approach^{9,10} at similar temperature and dopant concentration. The critical concentration N_c for the MNM transition is deduced from the results and compared with previous estimates obtained from three different computational methods.

II. EXPERIMENTAL DETAILS

All samples considered in this work were nitrogen-doped 4H-SiC epitaxial layers grown at CEA-LETI (France) in a home-made chemical vapor deposition reactor. They have been already characterized in much detail, from the optical, electrical, and structural point of view. This included the realization of Schottky diodes with forward current density equals to 60 A/cm² and an ideality factor very close to 1, as well as prototype Hall sensors working from room tempera-

TABLE I. Summary of sample structure, doping level, and layer thickness of the eight different samples considered in this work.

Sample	Structure	Doping (cm ⁻³)	Thickness (μm)
1	<i>n/p/n</i>	$3.5 \times 10^{15}/2 \times 10^{15}/8 \times 10^{18}$	2.4/3.5/350
2	<i>n/p/n</i>	$5.2 \times 10^{16}/2 \times 10^{15}/8 \times 10^{18}$	0.6/3.5/350
3	<i>n/p/n</i>	$1.38 \times 10^{17}/2 \times 10^{15}/8 \times 10^{18}$	0.5/3.5/350
4	<i>n/p/n</i>	$2.2 \times 10^{17}/2 \times 10^{15}/8 \times 10^{18}$	0.6/3.5/350
5	<i>n/p</i>	$7.5 \times 10^{17}/8.5 \times 10^{17}$	1/350
6	<i>n/p</i>	$1 \times 10^{19}/8.5 \times 10^{17}$	0.15/350
7	<i>n/p</i>	$4 \times 10^{19}/8.5 \times 10^{17}$	0.4/350
8	<i>n/p</i>	$5 \times 10^{19}/8.5 \times 10^{17}$	0.5/350

ture to 800 K. For more details, see Refs. 11 and 12. In this work, different eight samples have been selected. They were *n* type, with nitrogen concentrations ranging from 3.5×10^{15} to 5×10^{19} cm⁻³. The detailed structure and doping levels have been listed in Table I. The electrically activated nitrogen density has been deduced from high-temperature Hall-effect measurements. The resistivity was determined from van der Pauw measurements performed on mesa-etched structures and, in order to carry experimental investigations in the temperature range 6–900 K, two different experimental setups were used.

At low temperature, we used a Keithley electrometer with an input resistance larger than 2×10^{14} Ω, paralleled by a 20-pF capacitance. Unfortunately, despite such a high input impedance, in the case of weakly doped samples we could not get reliable results below 40 K. This is why no experimental data are shown at low temperature in the case of samples 1–5. For the higher temperatures, we used the second setup with a home-made furnace operated under He gas atmosphere. In this case the experimental investigation range was 300–1000 K, only limited by contact failures.

III. TEMPERATURE DEPENDENCE OF THE RESISTIVITY

In the remaining part of this work, we divide our set of samples in two different series: first, samples 1–5 with a

large temperature dependence of the resistivity. This is typical of nitrogen concentrations below N_c . The second series contains samples 6–8 with a low-temperature dependence of the resistivity, which is now typical of nitrogen concentrations above N_c . This is shown in Fig. 1(a). For completeness, we display the resistivity vs temperature behavior of two representative samples per series.

A. Nitrogen concentrations below N_c

This first series of samples has been investigated in detail in the work of Ref. 5. The electrical behavior is standard and can be easily understood in the light of the textbook expression

$$\rho = \frac{1}{Ne\mu_n}, \quad (1)$$

in which ρ is the resistivity, N is the free-electron density, μ_n is the drift mobility, and e is the electron charge. Of course, all three quantities (ρ , N , and μ_n) vary as a function of the temperature T , donor density N_d , and compensation N_a . Given a temperature, to find N one must solve the neutrality equation for a given set of N_d and N_a concentrations:

$$N_d = N + N_u + N_a, \quad (2)$$

in which N_u represents the density of unionized donors. An important point to notice is that, in SiC polytypes, the situation is far more complex than the one already encountered in GaAs,¹³ or even Si.^{10,14} Indeed, nitrogen is known to substitute for carbon, but different (nonequivalent) C-lattice sites may coexist. In 4*H*-SiC, this results in two different ionization energies, which depend on the exact position of the nitrogen donor in the C sublattice. They have been termed hexagonal (*h*) and cubic (*k*) and the hexagonal sites give a shallower level (~60 meV) than the cubic ones (~90 meV). Moreover, because of the indirect band structure, both experience valley-orbit splitting. The complete model should then include one (compensating) acceptor level, two fundamental donor levels, and two excited states. All are below the conduction band and the *n*-type carriers will be distributed between them and the continuum states

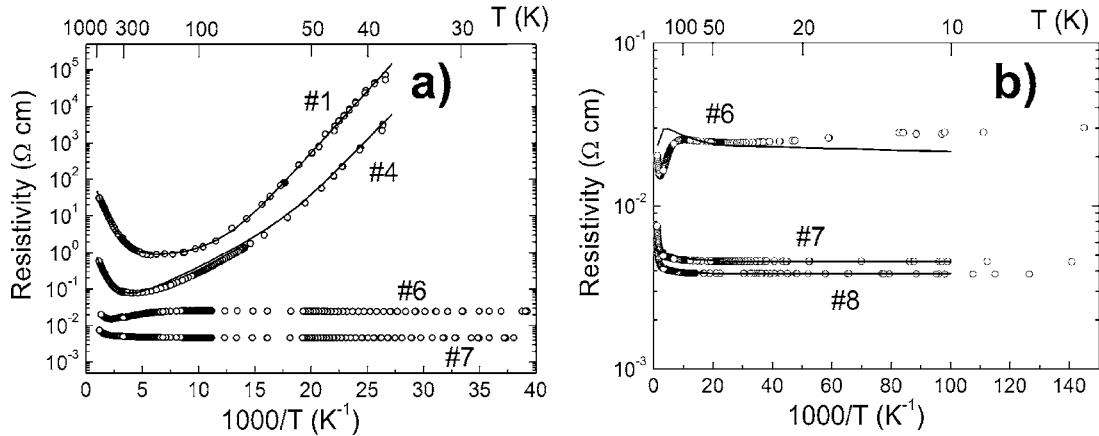


FIG. 1. Change in electrical resistivity for nitrogen-doped 4*H*-SiC epitaxial layers vs $1000/T$. (a) Samples 1, 4, 6, and 7 for $25 < T < 900$ K; (b) samples 6, 7, and 8 for $6 < T < 900$ K. The solid lines are theoretical fits as explained in the text.

according to the Fermi-Dirac distribution function. For more details, see Ref. 5.

Of course, having two very different ionization energies is very interesting because incidentally the shallower h -site level can be fully ionized before the deeper k -site electrons become electronically active, especially at low temperature. These free “ h -site electrons” screen the bounded and localized k -state electrons, and thereby facilitate the ionization of the deeper state. Therefore the average ionization energy for full ionization (i.e., when all electrons are conducting) lies between 60 and 90 meV, but closer to 60 meV. This is why the slope on the measured resistivity curves shown in Fig. 1(a) is only weakly concentration dependent. As a matter of fact, and because the mobility is almost constant up to 100 K,^{4,5} it corresponds mainly to the ionization of the shallowest “ h -site” level.

Above 100 K the situation becomes more complicated. A competition between the variation of N and μ_n gives, first, a minimum and, then, an increase in the final resistivity. Indeed, from one side the carrier concentration increases with the temperature up to the exhaustion regime. Then, above a critical temperature which depends of the donor density and compensation, it remains constant. At the same time, the mobility decreases with a power law which comes from phonon scattering and the resistivity increases. This behavior results in the final temperature dependence shown as full lines in Fig. 1(a) for sample 1 and sample 4. For more details, see again Ref. 5.

B. Nitrogen concentration above N_c

In this case, the temperature dependence of the resistivity (shown for sample 6 and sample 7) in Fig. 1(a) displays a totally different behavior. There is no thermal activation at low temperature, which clearly indicates a metallic character with fairly constant mobility. This is exactly what should be expected from the consideration of experimental results collected for bismuth-doped silicon in the work of Ref. 10. Notice also that, similar to Bi-doped Si, there is a weak indication of a semiconductorlike behavior above 100 K for sample 6. This is shown in more detail in Fig. 1(b) and, from Table I, sets clearly the MNM transition in $4H$ -SiC at $\sim 10^{19}$ cm⁻³. Of course, in this case the transport properties could not be explained using the relaxation time approximation as run in Ref. 5. A totally different approach is needed. This is done in this work.

IV. THEORY

We work in the light of the generalized Drude approach (GDA) method⁹ as previously used to determine the resistivity and the critical concentration of the shallow double-donor system Si:Bi,P.¹⁴ This approach, in which the generalization of the Drude expression consists of allowing the relaxation time to be frequency dependent, works well for a dominant impurity scattering and consists of three steps. In the first step the high-frequency limit of the dynamical conductivity

is derived within the Kubo formalism and a diagrammatic perturbation theory. In the second step, this result is compared to the high-frequency expansion of the generalized Drude expression for the dynamical conductivity and the relaxation time τ is hereby identified. Finally, in the third and last step, the expression obtained for τ is assumed to be valid at zero frequency.

Since, basically, the calculation neglects the electron-lattice interaction it is not expected to be accurate in the low concentration range. The calculation can still be run, but the results reflect only the degree of ionization of the impurities. Furthermore, since the calculation is not expected to be accurate, we can safely neglect the effect of valley-orbit splitting and compensation. Compensation, for instance, would lead to a lower carrier concentration and a higher density of scattering centers. Similar to the electron-lattice interaction, this would increase the resistivity.

We assume simply that the total concentration of nitrogen atoms is given by $N_{d1}=N_{d2}=N_d/2$ and calculate the energy of the resulting modes ($E_{I,i}$) with relative weights χ_i . The imaginary part of the inverse dielectric function has two peaks, corresponding to excitations from the two levels.¹⁴ The relative weights are defined as the relative areas of the two peaks. Above the critical concentration N_c , we assume that all donor are ionized. Below the MNM, at a finite temperature T , only part of the doping species are ionized. The rest remains neutral. In this case, to compute the density of free carriers in the nonmetallic regime, we solve simultaneously the two equations:

$$N_d = N + N_u, \quad (3)$$

$$N_u = N_d \left(\frac{\chi_1}{e^{[E_{I,1}-\mu(N,T)]\beta} + 1} + \frac{\chi_2}{e^{[E_{I,2}-\mu(N,T)]\beta} + 1} \right), \quad (4)$$

in which $E_{I,i}(i=1,2)$ is the ionization energy for a single donor of type i , $\beta=1/(k_B T)$ with k_B being the Boltzmann's constant and $\mu(N,T)$ is the chemical potential.

The important point to outline is that this model neglects the effect of valley-orbit splitting and compensation, but still includes two localized (hexagonal and cubic) donor levels below the conduction band. Of course, below N_c the carriers remain distributed among them and the continuum of the conduction band according to the Fermi-Dirac distribution function.

To compute the resistivity ρ , we notice that in a polar semiconductor the static resistivity is the same as the one in a nonpolar semiconductor, while in the nonpolar case the computation is far simpler. Since we are only interested in the static results, and since even in this case we do not want to perform a detailed quantitative comparison, we shall restrict ourselves to the expression of the resistivity in a nonpolar material:¹⁵

$$\rho(\omega) = \frac{-im^* \omega}{Ne^2} + \frac{i2}{3\pi N \omega} \int_0^\infty q^2 \left(\frac{1}{\epsilon_{tot}(q, \omega)} - \frac{1}{\epsilon_{tot}(q, 0)} \right) dq, \quad (5)$$

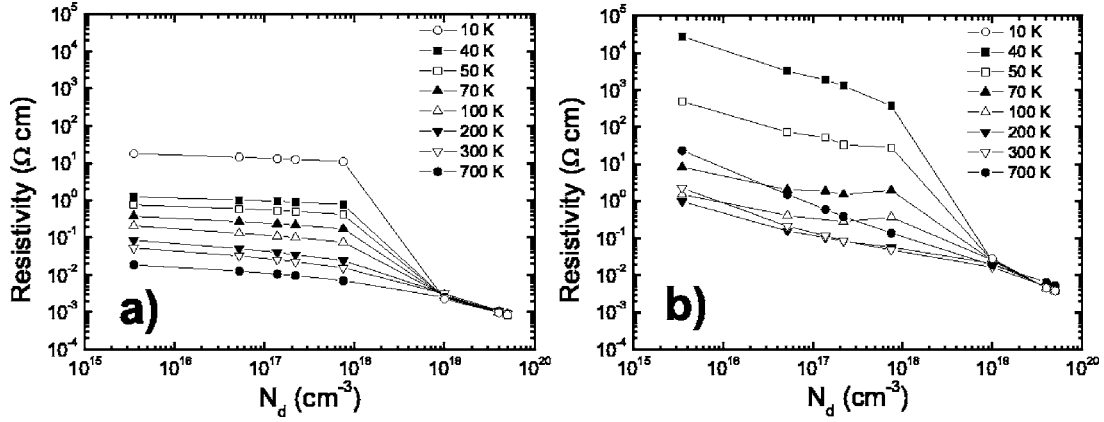


FIG. 2. Change in resistivity vs nitrogen donor concentration N_d (a) calculated from the generalized Drude approach and (b) measured in this work.

where m^* is the effective mass and ϵ_{tot} is the total dielectric function. As usual, we assume a random distribution of Coulomb impurities. The total dielectric function is given by^{16,17}

$$\epsilon_{tot}(q, \omega) = \epsilon + \nu\alpha_1(q, \omega) + i\nu\alpha_2(q, \omega). \quad (6)$$

In this expression, ϵ is the high-frequency dielectric constant of 4H-SiC while α_1 and α_2 are the real and imaginary parts of the polarizability of the dopant carriers from one of the $\nu=3$ valleys of the conduction-band minimum at the M point. We take for the dielectric constant $\epsilon = (2\epsilon_{\perp} + \epsilon_{\parallel})/3 = 9.78$ and for the geometric average of the effective mass $m^* = (m_x m_y m_z)^{1/3} = 0.37m_0$.⁷ For the hexagonal and cubic ionization energies in 4H-SiC, we take 91.8 and 52.1 meV.¹⁸ Finally, in the random-phase approximation (RPA), we compute the imaginary part of the dopant-carrier polarizability from the analytic expression:

$$\alpha_2(Q, W) = \frac{-m^* e^2}{8\hbar^2 k_F Q^3 B} \times \left[\ln \left(\frac{\cosh\{B[W + (Q^2 + W^2/Q^2 - M)/2]\}}{\cosh\{B[W - (Q^2 + W^2/Q^2 - M)/2]\}} \right) - 2BW \right], \quad (7)$$

in which we have introduced four dimensionless variables: $Q = q/(2k_F)$, $W = \hbar\omega/(4E_F)$, $B = \beta E_F$, and $M = \mu/E_F$. The quantity $k_F = (3N\pi^2)^{1/3}$ is the Fermi wave vector and E_F is the Fermi energy.

The real part of the polarizability can be obtained from the imaginary part through the Kramers-Kronig dispersion relation. Since we are interested in the static resistivity, this can be written as

$$\rho(0) = \frac{16\hbar k_F^3}{12\pi N E_F} \int_0^{\infty} Q^2 \frac{[\partial\alpha_2(Q, W)/\partial W]_{W=0}}{[\epsilon + \alpha_1(Q, 0)]^2} dQ, \quad (8)$$

which can be reduced to

$$\rho(0) = \frac{2(m^* e)^2}{3\pi N \hbar^3} \int_0^{\infty} \frac{1 - \tanh[0.5B(Q^2 - M)]}{Q[\epsilon + \alpha_1(Q, 0)]^2} dQ. \quad (9)$$

Finally, the chemical potential μ is obtained from the implicit expression

$$B^{3/2} = \int_0^U \frac{3y}{1-y^2} \left[A + \ln \left(\frac{1-y^2}{y^2} \right) \right]^{1/2} dy, \quad (10)$$

where $U = (1 + e^{-A})^{-1/2}$ and $A = BM = \mu B$. For a given A , one obtains B leading to a relation between them.

V. DISCUSSION

The calculated values of the resistivity of 4H-SiC as a function of the impurity concentration and temperature are shown in Fig. 2(a). They are compared to the experimental values in Fig. 2(b). Notice that both experimental and theoretical curves present the same range of donor concentrations and temperature. Notice also that they have very similar forms. Since they are both converging to the same (almost temperature-independent) behavior around 10^{19} cm^{-3} , we confirm that this is the critical concentration N_c for the MNM transition in 4H-SiC.

As expected, there is some quantitative difference between the series of experimental and theoretical data. At low temperature, and for the lowest doped sample, this can amount to three orders of magnitude. As already said, this comes simply because we neglected in the GDA calculation the effect of compensation, lattice interaction, and neutral impurity scattering. When properly taken into account in the description of scattering, the discrepancy disappears.⁵ This was already shown in Fig. 1(a) for samples 1 and 4. A similar discrepancy remains above N_c , but much less important. This is shown in Fig. 1(b) for samples 6–8. Using the theoretical values computed in Fig. 2(a) to represent the GDA variation of resistivity in the temperature range 10–700 K (full lines), we find a scaling factor of only 10 for sample 6 which reduces to 4.5 above N_c (samples 7 and 8).

Previously, theoretical determinations of N_c were done in the work of Ref. 7. Comparing the total energy of the electron gas with the total energy of the electrons in a nonmetallic phase, Persson *et al.* estimated N_c to be around $5.6 \times 10^{18} \text{ cm}^{-3}$. This value is very close to the one given by the

Mott ($5.5 \times 10^{18} \text{ cm}^{-3}$) and Mott-Hubbard ($5.6 \times 10^{18} \text{ cm}^{-3}$) approximations, modeled from overlapping impurity electrons assuming hydrogenlike wave functions. The earlier many-particle method used to determine the MNM critical concentration was based on static total-energy calculations for $T=0$ K, modeling the material for two limits: low doped and heavily doped, and finding an intersecting point of the total energies. Earlier $N_c=10^{19} \text{ cm}^{-3}$ was thus a $T=0$ K value. The present many-particle method is a temperature-dependent model of the electronic current, describing a dynamic property. The earlier and present methods are complementary. However, the present method is more direct, and can be compared to resistivity measurement which is a great advantage. The other methods described the electronic structure more accurately. The present resistivity measurements, together with the temperature-dependent GDA calculation and the comparison with values obtained from the relaxation time approximation, constitute real determination of the MNM transition in 4H-SiC. In this way, we got $N_c \sim 10^{19} \text{ cm}^{-3}$.

VI. CONCLUSION

To summarize, the temperature dependence of the resistivity for nitrogen-doped 4H-SiC has been investigated for concentrations which span the insulating to metallic regimes. Experimental results collected between 10 and 700 K have been compared with the results of a generalized Drude approach. At high doping level, a good qualitative agreement has been obtained and the value of the critical impurity concentration N_c for the MNM transition has been estimated to be 10^{19} cm^{-3} .

ACKNOWLEDGMENTS

We wish to thank E. Neyret T. Billon, and L. Di Cioccio (LETI-CEA in Grenoble, France) for providing us with the series of samples investigated in this work. One of us, C.P., acknowledges support from the Swedish Research Council (VR). Another of us (A.F.S.) thanks the Brazilian Research Council (CNPq) for financial support.

*Electronic address: julien.pernot@grenoble.cnrs.fr

¹For a recent review on SiC electronic devices, see *Silicon Carbide: Recent Major Advances*, edited by W. J. Choyke, H. Matsunami, and G. Pensl (Springer, Berlin, 2004), pp. 737–868.

²See, for instance, A. Loyd-Spetz and S. Savage, in *Silicon Carbide: Recent Major Advances* (Ref. 1), pp. 869–896.

³J. L. Robert, S. Contreras, J. Camassel, J. Pernot, E. Neyret, and L. Di Cioccio, *Sens. Actuators, A* **97-98C**, 27 (2002).

⁴J. Pernot, S. Contreras, J. Camassel, J. L. Robert, W. Zawadzki, E. Neyret, and L. Di Cioccio, *Appl. Phys. Lett.* **77**, 4359 (2000).

⁵J. Pernot, W. Zawadzki, S. Contreras, J. L. Robert, E. Neyret, and L. Di Cioccio, *J. Appl. Phys.* **90**, 1869 (2001).

⁶J. Pernot, J. Camassel, H. Peyre, S. Contreras, and J. L. Robert, *Mater. Sci. Forum* **433-436**, 403 (2003).

⁷C. Persson, U. Lindefelt, and Bo E. Sernelius, *Phys. Rev. B* **60**, 16479 (1999).

⁸C. Persson and A. Ferreira da Silva, in *Optoelectronic Devices: III-Nitrides*, edited by M. Razeghi and M. Henini (Elsevier, Oxford, 2004), pp. 479–559.

⁹Bo E. Sernelius, *Phys. Rev. B* **40**, 12438 (1989); **36**, 1080

(1987).

¹⁰E. Abramof, A. Ferreira da Silva, Bo E. Sernelius, J. P. de Souza, and H. Boudinov, *Phys. Rev. B* **55**, 9584 (1997).

¹¹E. Neyret, L. Di Cioccio, J. M. Bluet, J. Pernot, P. Vicente, D. Anglos, M. Lagadas, and T. Billon, *Mater. Sci. Eng., B* **80**, 332 (2001).

¹²J. L. Robert, S. Contreras, J. Camassel, J. Pernot, S. Juillaguet, L. Di Cioccio, and T. Billon, *Mater. Sci. Forum* **389-393**, 1435 (2002).

¹³A. Ferreira da Silva, I. Pepe, Bo E. Sernelius, C. Persson, R. Ahuja, J. P. de Souza, Y. Suzuki, and Y. Yang, *J. Appl. Phys.* **95**, 2532 (2004).

¹⁴A. Ferreira da Silva, Bo E. Sernelius, J. P. de Souza, H. Boudinov, H. Zheng, and M. P. Sarachik, *Phys. Rev. B* **60**, 15824 (1999).

¹⁵Bo E. Sernelius and M. Morling, *Thin Solid Films* **177**, 69 (1989).

¹⁶R. Sirko and D. L. Mills, *Phys. Rev. B* **18**, 4373 (1978).

¹⁷Bo E. Sernelius, *Thin Solid Films* **208**, 96 (1992).

¹⁸W. Götz, A. Schöner, G. Pensl, W. Suttrop, W. J. Choyke, R. Stein, and S. Leibenzeder, *J. Appl. Phys.* **73**, 3332 (1993).